Commun. Comput. Phys.
doi: 10.4208/cicp.090310.020610a

Vol. **x**, No. x, pp. 1-21
xxx 2010

Numerical Study of Surfactant-Laden Drop-Drop Interactions

Jian-Jun Xu[1,*], Zhilin Li[2], John Lowengrub[3] and Hongkai Zhao[3]

[1] *School of Mathematical and Computational Sciences, Xiangtan University, Xiangtan, Hunan 411105, China.*
[2] *Department of Mathematics, North Carolina State University, Raleigh, NC, 27695, USA.*
[3] *Department of Mathematics, University of California Irvine, Irvine, CA, 92697, USA.*

Received xx xxxx; Accepted (in revised version) xx xxxx

Communicated by Pingwen Zhang

Available online xxx

Abstract. In this paper, we numerically investigate the effects of surfactant on drop-drop interactions in a 2D shear flow using a coupled level-set and immersed interface approach proposed in (Xu et al., J. Comput. Phys., 212 (2006), 590–616). We find that surfactant plays a critical and nontrivial role in drop-drop interactions. In particular, we find that the minimum distance between the drops is a non-monotone function of the surfactant coverage and Capillary number. This non-monotonic behavior, which does not occur for clean drops, is found to be due to the presence of Marangoni forces along the drop interfaces. This suggests that there are non-monotonic conditions for coalescence of surfactant-laden drops, as observed in recent experiments of Leal and co-workers. Although our study is two-dimensional, we believe that drop-drop interactions in three-dimensional flows should be qualitatively similar as the Maragoni forces in the near contact region in 3D should have a similar effect.

PACS: 47.55.D-, 47.55.dk, 47.55.N-

Key words: Surfactants, drops, coalescence, surface tension, Marangoni effect, level-set method, immersed interface method, Stokes flow.

1 Introduction

The microstructure of emulsions and polymer blends depends strongly on the coalescence events that occur during processing. Surfactants and compatibilizers (block copolymers) are often used to prevent coalescence events and stabilize drop size distributions.

*Corresponding author. *Email addresses:* jjxu21@xtu.edu.cn (J. Xu), zhilin@math.ncsu.edu (Z. Li), lowengrb@math.uci.edu (J. Lowengrub), zhao@math.uci.edu (H. Zhao)

Flow induced coalescence of drops in a viscous fluid has historically been modeled and described as taking place in three consecutive stages (see e.g., [7,12,15,19]). The first stage is the approach and collision of drops, starting from an initially large separation. The second stage is film drainage, which commences when the separation distance is asymptotically small compared to the drop radii. During this stage, the relative translational motion of the drops is largely arrested, and the motion consists of rotation of the two-drop pair in the flow, with simultaneous thinning of the thin film that separates the two drops. As the film thins, the distance between the two drops may become small enough for non-hydrodynamic attractive forces such as van der Waals attractive force to trigger an instability leading to film rupture. When this occurs, this third stage leads rapidly to coalescence. The theory of film drainage for clean drops was reviewed by Chesters [3]. In the absence of van der Waals forces, the interacting drops reach a minimum distance as a consequence of a balance of the compressional force imposed by the flow and the repulsive lubrication force in the thin film separating the drops. The drops then separate without coalescing. Coalescence therefore requires non-hydrodynamic forces such as the van der Waals force to rupture the film when the film is sufficiently thin.

The presence of surfactants introduces three main mechanisms during the drop interactions: the average reduction in surface tension associated to the presence of surfactants; nonuniform capillary pressure (normal stresses) on the drop surface due to non-uniform distribution of surfactants; Marangoni forces associated variation of surface tension along the interface.

The effect of surfactants on drop-drop collisions and coalescence has been investigated theoretically (e.g., [4, 5, 29]) and experimentally (e.g., [7, 12, 15, 19, 26, 47]). In a series of experiments, Leal and co-workers [12,15,19,47] found that surfactants can have surprising and non-monotonic effects on the coalescence of two drops for a wide range of viscosity ratios. In particular, for a small amount of surfactants, the critical Capillary number below which coalescence occurs decreases significantly compared to that for clean drops. When additional surfactant is added, the critical Capillary number increases towards that for clean drops. Further, a range of Capillary numbers, with a nonzero lower bound, is found for which coalescence occurs. When the initial offset of the drops is above a critical threshold, no coalescence is found below or above this range.

There has been much work on simulating the motion of a single surfactant-laden drop (or bubble) using various numerical methods including boundary integral (e.g., [2,9,23, 28,33,38]), volume of fluid (e.g., [8,13,20]), arbitrary Lagrangian-Eulerian (e.g., [10,11, 46]), front tracking (e.g., [16,17,30,39,48]), level-set [25,43,44], and diffuse interface [1,40] methods. However there are few numerical studies on surfactant-laden drop-drop interactions. Recently, Dai and Leal [7] used a boundary integral method to study head-on collisions of surfactant-laden drops in a biaxial extensional flow. In addition to finding that the interface is immobilized in the near contact region, they also found that the hydrodynamic force pushing the drops together is increased by the Marangoni immobilization of the interface outside of the thin film of fluid separating the drops. This causes

the drop to be much more deformed than it is in the absence of surfactant at the same Capillary number, and the more dimpled drop shapes slow the rate of film drainage in the near contact region.

In this paper, we investigate the collisions of two-dimensional surfactant-laden drops using a coupled level-set and immersed interface approach recently proposed in [44]. The interface evolution is captured using a level-set formulation where the interface is defined as the zero level-set of an auxiliary (level-set) function. The immersed interface method is used to obtain accurate solutions to the Stokes equations that govern the motion of the fluid in the presence of an interface. The surfactant dynamics are posed using an Eulerian formulation for solving partial differential equations on a moving interface. We focus on shear flow which is very important in blend processing and we do not consider van der Waals forces so that rupture of the thin film and drop coalescence do not occur. Instead, we investigate the characteristic behavior of the drops during their interaction by studying the minimum distance between them as well as the resulting hydrodynamic diffusion, as an additional measure of drop separation, as functions of parameters that control the strength of the flow and the surfactant coverage and dynamics. Interestingly, we find that there are non-monotonic conditions for coalescence of surfactant-laden drops as in the experiments of Leal and co-workers discussed above.

The paper is organized as follows. We first present mathematical formulation in Section 2. The numerical methods are briefly described in Section 3. Simulation results are presented in Section 4. Finally, conclusions and future work are given in Section 5.

2 Formulation

2.1 Dimensional equations

We consider a pair of equal-sized drops of radius a and viscosity μ_d placed in an matrix fluid with viscosity μ_m. Let Ω_i, with $i=d,m$, be the domains occupied by the drops and matrix fluid respectively. Let $\Omega=\Omega_d\cup\Omega_m$, Σ be the interface separating the drops and matrix, and $\partial\Omega$ be the fixed outside boundary of Ω. In this paper, we assume for simplicity that the densities and viscosities for the two fluids (i.e., drop and matrix) are matched: $\rho_d=\rho_m=\rho$ and $\mu_d=\mu_m=\mu$. We also assume that the far-field flow velocity is a simple shear, i.e., $\mathbf{u}_\infty=\dot{\gamma}y\mathbf{e}_x$, where $\mathbf{e}_x$ is the coordinate vector in the x-direction and $\dot{\gamma}$ is the shear rate. We further neglect inertial effects. Consequently, the Stokes equations govern the motion of the drop and matrix fluids:

$$\nabla\cdot\mathbf{T}=0,\quad \nabla\cdot\mathbf{u}=0,\quad \text{in } \Omega, \tag{2.1}$$

where $\mathbf{T}=-pI+\mu(\nabla\mathbf{u}+\nabla\mathbf{u}^T)$ is the stress tensor, and p is the pressure. Across the interface Σ, the velocity is continuous, and the Laplace-Young jump condition holds [18]:

$$[\mathbf{Tn}]_\Sigma\equiv\mathbf{Tn}|_{\Sigma,m}-\mathbf{Tn}|_{\Sigma,d}=\sigma\kappa\mathbf{n}-\nabla_s\sigma, \tag{2.2}$$

where σ is the surface tension coefficient, $\mathbf{n}$ is the normal vector to Σ directed towards the matrix fluid, $\kappa=\nabla\cdot\mathbf{n}$ is the curvature of Σ (positive for spherical/circular interfaces) and $\nabla_s=(I-\mathbf{n}\otimes\mathbf{n})\nabla$ is the surface gradient. $\nabla_s\sigma$ is the Marangoni force, and $-\sigma\kappa\mathbf{n}$ is the Capillary force.

The interface moves with velocity $\mathbf{u}$:

$$\frac{d\mathbf{x}}{dt}=\mathbf{u}. \tag{2.3}$$

When surfactants are present, the Langmuir equation of state (EOS) [33] is often used to describe the relation between the surfactant concentration f and the surface tension σ:

$$\sigma(f)=\sigma_0+RTf_\infty\log\Big(1-\frac{f}{f_\infty}\Big), \tag{2.4}$$

where σ_0 is the surface tension for a clean interface ($f=0$), f_∞ is the surfactant concentration at maximum packing, R is the ideal gas constant, and T is the absolute temperature.

Here, we consider insoluble surfactants. Surfactants are then convected and diffused along the interface. The surfactant concentration, f, satisfies [13, 44]

$$f_t+\mathbf{u}\cdot\nabla f-\big(\mathbf{n}\cdot\nabla\mathbf{u}\cdot\mathbf{n}\big)f=D_s\nabla_s^2 f, \tag{2.5}$$

where D_s is the surfactant (surface) diffusivity. See also [37, 41, 45] for other forms of Eq. (2.5).

2.2 Nondimensionalization

Using the nondimensionalization given in [2, 13, 44], where the drop radius a is used as the length scale and the inverse shear rate $\dot\gamma^{-1}$ for time is used as the time scale, the nondimensional Stokes system is

$$\Delta\mathbf{u}=\nabla p,\quad \nabla\cdot\mathbf{u}=0,\quad \text{in }\ \Omega, \tag{2.6}$$

together with interface conditions

$$[\mathbf{u}]_\Sigma=0,\qquad [\mathbf{Tn}]_\Sigma=\frac{1}{Ca}(\sigma\kappa\mathbf{n}-\nabla_s\sigma), \tag{2.7}$$

where $Ca=\mu a\dot\gamma/\sigma_e$ is the Capillary number, $\sigma_e=\sigma(f_e)$ is the effective surface tension, and

$$f_e=\frac{1}{|\Sigma_0|\int_{\Sigma_0}f_0 d\Sigma},$$

where Σ_0 is the initial position of the interface and f_0 is the initial surfactant concentration. The nondimensional surface tension σ is

$$\sigma(f)=\frac{1+E\ln(1-xf)}{1+E\ln(1-x)}, \tag{2.8}$$

where $E=RTf_\infty/\sigma_0$ is the surfactant elasticity and x is the surfactant coverage $x=f_e/f_\infty$. The nondimensional equation for surfactant is the same as Eq. (2.5) with D_s replaced by $1/Pe$, where $Pe=a^2\dot{\gamma}/D_s$ is the Peclet number.

The Stokes equations can be further written as the following Poisson equations for the pressure [22]

$$\nabla^2 p=0, \quad \text{in } \Omega, \tag{2.9}$$

with jump boundary conditions on Σ

$$[p]_\Sigma=-\frac{1}{Ca}\sigma\kappa, \qquad \left[\frac{\partial p}{\partial n}\right]_\Sigma=\frac{1}{Ca}\nabla_s^2\sigma, \tag{2.10}$$

and the Neumann boundary condition

$$\frac{\partial p}{\partial n}=\nabla^2\mathbf{u}\cdot\mathbf{n}, \quad \text{on } \partial\Omega, \tag{2.11}$$

and the velocity

$$\nabla^2\mathbf{u}=\nabla p, \quad \text{in } \Omega, \tag{2.12}$$

together with the jump boundary conditions

$$[\mathbf{u}]_\Sigma=0, \qquad \left[\frac{\partial \mathbf{u}}{\partial n}\right]_\Sigma=-\frac{1}{Ca}\nabla_s\sigma, \tag{2.13}$$

and the far-field Dirichlet boundary condition

$$\mathbf{u}=y\mathbf{e}_x, \quad \text{on } \partial\Omega. \tag{2.14}$$

2.3 Interface representation

Following [44], the level-set method, first introduced by Osher and Sethian [32], is used to represent the interface implicitly using an auxiliary (level-set) function ϕ, e.g., $\Sigma(t)=\{\mathbf{x}|\phi(\mathbf{x},t)=0\}$, such that

$$\phi_t+\mathbf{u}\cdot\nabla\phi=0. \tag{2.15}$$

This approach has been highly successful describing interface dynamics in many applications including multiphase flows. See the recent reviews [31,34], for example.

In practice, we use two level-set functions, one for each drop, to avoid kinks in the level-set function in the near contact region between the two drops when a single level-set function is used, see e.g., [27,44]. Further, at every time step, the level-set function ϕ is re-initialized to be a distance function, e.g., $|\nabla\phi|\approx 1$, by solving the Hamilton-Jacobi equation [36]

$$\begin{cases} \phi_\tau+S(\phi_0)(|\nabla\phi|-1)=0, \\ \phi(\mathbf{x},0)=\phi_0(\mathbf{x}), \end{cases} \tag{2.16}$$

where ϕ_0 is the level-set function before the re-initialization, τ is the pseudo-time and $S(x)$ is the sign function of x defined as

$$S(x)=\begin{cases} -1, & \text{if } x<0, \\ 0, & \text{if } x=0, \\ 1, & \text{if } x>0. \end{cases} \tag{2.17}$$

Geometrical quantities can be easily computed using level-set function. Assume that $\{\mathbf{x}:\phi(\mathbf{x},t)<0\}=\Omega_d$, then the outward normal vector and total curvature are

$$\mathbf{n}=\frac{\nabla\phi}{|\nabla\phi|}, \qquad \kappa=\nabla\cdot\Big(\frac{\nabla\phi}{|\nabla\phi|}\Big). \tag{2.18}$$

Finally, since the surfactant equation is solved on a Cartesian mesh around the interface, the surfactant field f is extended off Σ at every time step by solving a liner convection equation [49]

$$\begin{cases} f_\tau+S(\phi)\mathbf{n}\cdot\nabla f=0, \\ f(\mathbf{x},0)=f_0(\mathbf{x}). \end{cases} \tag{2.19}$$

See [44] for further details.

3 Numerical methods

In this section we briefly describe the numerical approach. The reader is referred to [44, 45] for further details. The standard third order upwinding WENO method [14] is used for the spatial discretization and the standard third order TVD Runge-Kutta method [35] is used for time marching for the level-set advection equation (2.15), and the Hamilton-Jacobi equations (2.16) and (2.19) for the re-initialization of the level-set function and for the extension of the surfactant field off Σ, respectively. Further, a smooth approximation of the signed distance function,

$$S_h(\phi)=\frac{\phi}{\sqrt{\phi^2+h^2}},$$

is used. To solve the surfactant transport equation (2.5), a second order accurate, semi-implicit time discretization is used to allow large time steps, $\Delta t=\mathcal{O}(h)$, following [44,45]. The key idea is to decompose

$$\nabla_s^2 f=\nabla^2 f-\frac{\partial^2 f}{\partial n^2}-\kappa\frac{\partial f}{\partial n},$$

where ∇^2 is the usual Cartesian Laplacian operator, and to treat ∇^2 using the Crank-Nicolson method, which can easily be inverted, and to use an explicit discretization (e.g.,

Adams-Bashforth) for the normal derivative and nonlinear terms [42, 45]

$$\frac{f^k-f^{k-1}}{\Delta t}=\frac{1}{2Pe}\left(\nabla^2 f^k+\nabla^2 f^{k-1}\right)+\frac{3}{2}\Big[-\frac{1}{Pe}\Big(\kappa\frac{\partial f}{\partial \mathbf{n}}+\frac{\partial^2 f}{\partial \mathbf{n}^2}\Big)-\mathbf{u}\cdot\nabla f+\mathbf{n}\cdot(\nabla \mathbf{u}\mathbf{n})f\Big]^{k-1}$$
$$-\frac{1}{2}\Big[-\frac{1}{Pe}\Big(\kappa\frac{\partial f}{\partial \mathbf{n}}+\frac{\partial^2 f}{\partial \mathbf{n}^2}\Big)-\mathbf{u}\cdot\nabla f+\mathbf{n}\cdot(\nabla \mathbf{u}\mathbf{n})f\Big]^{k-2}, \tag{3.1}$$

where $f^k\approx f(\mathbf{x},t)$ at time $t=t_k$. Standard center difference schemes are used for space discretization except that the third order WENO scheme [14] is used for the convection term $\mathbf{u}\cdot\nabla f$. All these equations are solved in small tubes around the drop boundaries.

The Stokes equations are solved using the Immersed Interface Method (IIM), introduced by LeVeque and Li [21, 22]. This method has become an increasingly popular choice for solving interface problems with jump discontinuities. The IIM is formally second order accurate and uses a Cartesian grid so that fast Poisson solvers (such as the FFT and the multigrid method) can be utilized. At time t_k in the IIM, the pressure p^k is obtained by solving

$$\nabla^2 p^k=0, \tag{3.2}$$

with jump boundary conditions on Σ^k:

$$[p^k]_{\Sigma^k}=-\Big(\frac{1}{Ca}\sigma\kappa\Big)^k, \qquad \Big[\frac{\partial p}{\partial n}\Big]_{\Sigma^k}=\Big(\frac{1}{Ca}\nabla_s^2\sigma\Big)^k, \tag{3.3}$$

and Neumann boundary conditions on $\partial\Omega$:

$$\Big(\frac{\partial p}{\partial n}\Big)^k=\begin{cases} 2(\nabla^2\mathbf{u}\cdot\mathbf{n})^{k-1}-(\nabla^2\mathbf{u}\cdot\mathbf{n})^{k-2}, & k\geq 2,\\ (\nabla^2\mathbf{u}\cdot\mathbf{n})^{k-1}, & k=1.\end{cases} \tag{3.4}$$

The velocity $\mathbf{u}^k$ is then obtained by solving

$$\nabla^2\mathbf{u}^k=\nabla p^k, \tag{3.5}$$

together with the jump boundary conditions on Σ^k:

$$[\mathbf{u}^k]_{\Sigma^k}=0, \qquad \Big[\frac{\partial \mathbf{u}^k}{\partial n}\Big]_{\Sigma^k}=-\Big(\frac{1}{Ca}\nabla_s\sigma\Big)^k, \tag{3.6}$$

and the far-field Dirichlet boundary condition

$$\mathbf{u}^k=y\mathbf{e}_x, \quad \text{on } \partial\Omega. \tag{3.7}$$

In the IIM, the grid points are then divided into two groups. All grid points that are adjacent to the interface classified as irregular grid points, while the remaining points are termed regular. At the regular grid points, the standard central difference scheme

is used to discretize the above Poisson equations. At the irregular grid points, the standard central difference scheme is modified by adding a correction term to account for the jumps. The interface position is obtained by an orthogonal projection of the irregular grid points to the interface. In order to approximate the jump conditions at the interface, the surfactant concentration (and surface tension) and its derivatives are computed at grid points in a local tube around the interface and are interpolated to the approximate interface position.

Finally, at each time step a small correction $\alpha\mathbf{n}$ is added to the velocity $\tilde{\mathbf{u}}_h$ computed by the IIM to enforce that the net mass flux across each drop interface is zero:

$$\int_\Sigma (\tilde{\mathbf{u}}_h + \alpha\mathbf{n})\cdot\mathbf{n}\,ds = 0,$$

where Ω is the region enclosed by the interface Σ. This yields the explicit expression

$$\alpha = -\frac{\int_\Sigma \tilde{\mathbf{u}}_h\cdot\mathbf{n}\,ds}{\int_\Sigma ds} = -\frac{\int \tilde{\mathbf{u}}_h\cdot\mathbf{n}\,\delta_\Sigma(\phi)\,d\mathbf{x}}{\int \delta_\Sigma(\phi)\,d\mathbf{x}}, \tag{3.8}$$

where δ_Σ is the surface delta function. This is performed for each drop and is an approach frequently used in boundary integral simulations (see e.g., [6]). The modified velocity is then used to evolve the level-set function and the surfactant concentration. We also multiply the surfactant concentration on each interface by a constant factor β to ensure that total surfactant mass is conserved. Let $\tilde{f}_h$ be the solution of Eq. (3.1), then β is determined by

$$\int_\Sigma \beta\tilde{f}_h\, d\Sigma = \int_{\Sigma_0} f_0 d\Sigma_0, \tag{3.9}$$

which yields

$$\beta = \frac{\int_{\Sigma_0} f_0\, d\Sigma_0}{\int_\Sigma \tilde{f}_h\, d\Sigma} = \frac{\int_\Omega f_0\delta_{\Sigma_0} d\mathbf{x}}{\int_\Omega \tilde{f}_h\delta_\Sigma d\mathbf{x}}. \tag{3.10}$$

The surfactant concentration is then reset to be $f_h = \beta\tilde{f}_h$. Finally, we note that other, more sophisticated area and surfactant concentration corrections can be derived that take into account the interface curvature and the surfactant concentration gradients. Nevertheless, we found it sufficient to use the simpler corrections described above. We refer the reader to [44,45] for numerical approximations of the delta function in the above integrals noting that $\delta_\Sigma = \delta(\phi)|\nabla\phi|$, where δ is the usual one-dimensional delta function.

4 Numerical results

In all our numerical simulations, the initial condition consists of two circular drops of unit radius centered at $(-1.7, 0.25)$ and $(1.7, -0.25)$ respectively. The initial surfactant concentration is uniform along the interface, i.e., $f(\mathbf{x},0) = 1$. Unless specified otherwise,

the computational domain is $[-7,7]\times[-5,5]$ and the number of grid points is $N_x=1400$ and $N_y=1000$ (correspondingly the grid size is $h=0.01$) and the time step $\Delta t=h/8$. Further, the Peclet number is taken to be $Pe=10$ and the surface elasticity is $E=0.2$.

4.1 Convergence study

To assess the accuracy of the algorithm, we perform a convergence study for several cases of drop interactions with surfactant. We use the minimum distance, $d_{\min}(Ca,x,h)$, between the two drops during the interaction to measure the convergence rate. The quantity $d_{\min}(Ca,x,h)$ is defined as follows. Let Σ_1,Σ_2 be the interfaces of two drops respectively, and t be time, then

$$d_{\min}(Ca,x,h)=\min_t \min_{\substack{\mathbf{x}_1\in\Sigma_1(t)\\ \mathbf{x}_2\in\Sigma_2(t)}} |\mathbf{x}_1-\mathbf{x}_2|. \tag{4.1}$$

In Table 1, the minimum distance $d_{\min}(Ca,x,h)$ is shown for several values of Ca and x, and for three mesh sizes. The minimum distance converges as the mesh is refined. The convergence rate shown in the table is estimated by solving

$$\frac{d_{\min}(Ca,x,h_2)-d_{\min}(Ca,x,h_1)}{d_{\min}(Ca,x,h_3)-d_{\min}(Ca,x,h_2)}=\frac{h_1^r-h_2^r}{h_2^r-h_3^r}, \tag{4.2}$$

for r, given the three mesh sizes h_1, h_2, h_3.

Table 1: Minimum distances between drops and predicted convergence rate.

	$x=0.3,Ca=0.06$	$x=0.2,Ca=0.04$
700×500	0.0765	0.0558
1400×1000	0.0804	0.0597
2100×1500	0.0807	0.0599
convergence rate	3.23	4.31

In Fig. 1, the relative errors in enclosed area (a) and surfactant mass (b) for one of the drops are plotted when $Ca=0.06$, $x=0.3$ using $N_x=1400$ and $N_y=1000$. The results for the other drop are analogous due to symmetry. The relative errors are seen to be less than 0.01% (10^{-4}) in each case. The corresponding corrections for the enclosed area α are less than 8% while those for the surfactant mass β are on the order of 0.01% (not shown).

Next, the pressure and surfactant concentration fields are shown in Fig. 2 at the critical time $t=7.66$ when the minimum distance achieved for the case with $Ca=0.06$, $x=0.3$. Observe in (a), (c), and (d) that the numerical pressure given by the immersed interface method is indeed discontinuous with the higher pressure being inside the drop. Also, note that the pressure has a local maximum in the near contact region of the matrix fluid due to lubrication forces. Observe in (b) that although the surfactant has accumulated at the drop tips, there is still some surfactant in the near contact region between the drops.

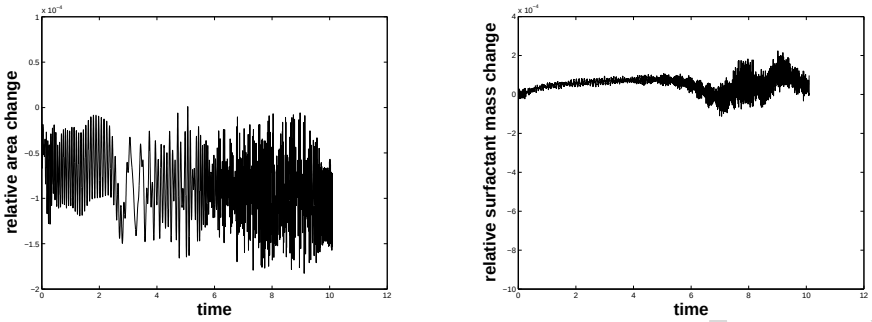

(a) (b)

Figure 1: The relative change in area enclosed by the drop (a) and in the surfactant mass (b) for the case $Ca=0.06$, $x=0.3$ using $N_x=1400$ and $N_y=1000$.

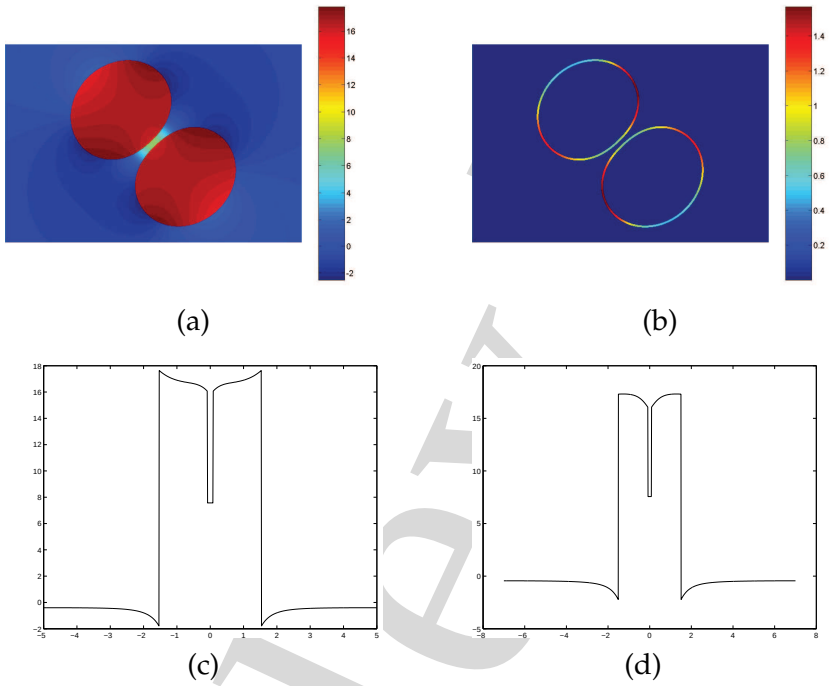

(a) (b)

(c) (d)

Figure 2: (a) The pressure contours for the case $Ca=0.06$, $x=0.3$ at time $t=7.66$; (b) The corresponding surfactant field at this time; (c) The $x=0$ slice of the pressure; (d) The $y=0$ slice of the pressure.

As can also be seen in the figure, gradients in pressure are associated with regions with rapidly varying surfactant distribution.

4.2 Examples of evolution with surfactant

We next consider drop-drop interactions with surfactant in further detail. In Figs. 3-5, three evolution sequences of the surfactant-laden drop-drop interactions are shown.

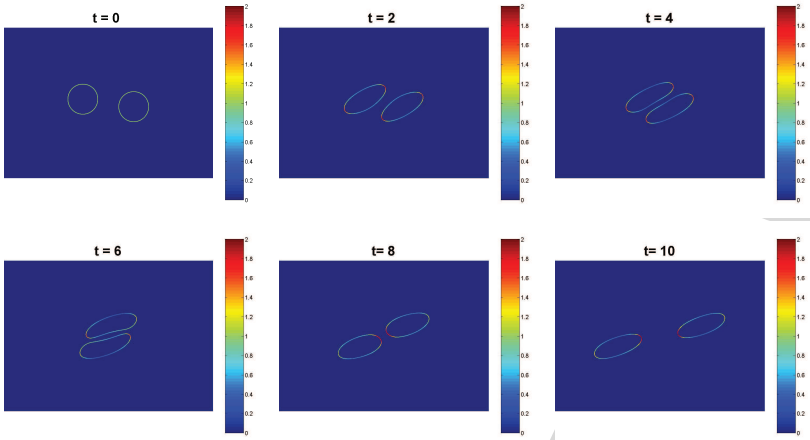

Figure 3: Contour plots of surfactant concentration. $x=0.3$, $Ca=0.5$.

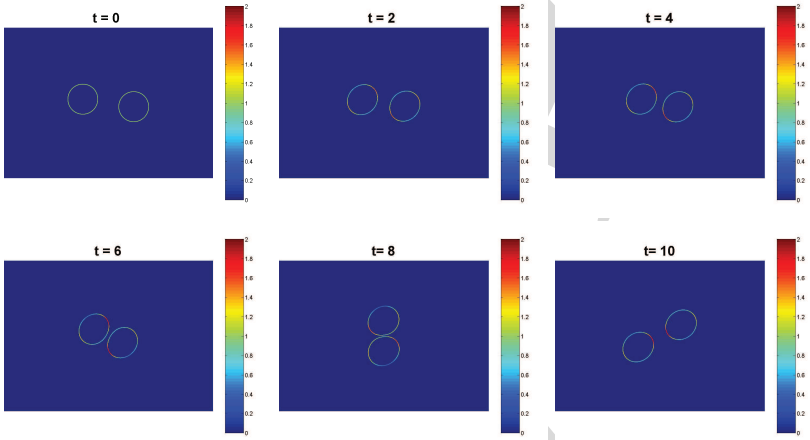

Figure 4: Contour plots of surfactant concentration. $x=0.3$, $Ca=0.06$.

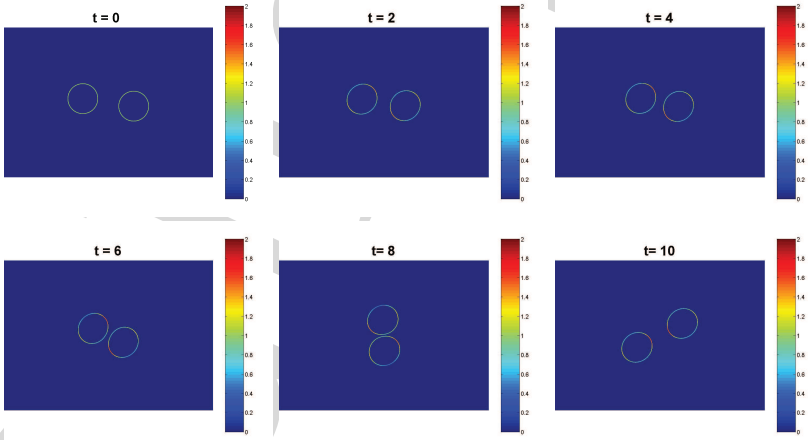

Figure 5: Contour plots of surfactant concentration. $x=0.3$, $Ca=0.04$.

Here, $x=0.3$ and Ca is varied. The contours of the surfactant concentration are plotted on the drop interfaces.

In Fig. 3, $Ca=0.5$ and the drops deform significantly due to the strength of the flow as they approach one another. Surfactant is initially swept to the drop tips. As the drops interact and rotate about one another, characteristic dimples form in the near contact region due to lubrication forces. The presence of the dimples makes it difficult to drain the fluid from the near contact region and the drops remain well-separated through the interaction process. In addition, during the interaction, surfactant at the leading edges of the drops is swept back to the trailing edges with a significant portion passing through the near contact region. As the drops separate, surfactant accumulates at the trailing edges of the drops resulting in a locally decreased surface tension. As a consequence of this and the development of a local straining flow in the separation region, the curvature at the trailing edges increases and the trailing edges elongate toward one another.

In Fig. 4, the Capillary number is decreased to $Ca=0.06$, simulating a weaker applied shear flow. In this case, the drops deform much less compared to the $Ca=0.5$ case shown in Fig. 3 and correspondingly, the drops approach one another more closely during their interaction. This is consistent with the case for clean drops where the minimum separation distance between drops is a monotonically increasing function of Ca [3] (e.g., smaller Ca yields smaller minimum distances).

In Fig. 5, the Capillary number is decreased even further to $Ca=0.04$. The drops deform only slightly as they interact and compared to the previous $Ca=0.5$ and $Ca=0.06$ cases, the surfactant distribution is more uniform with a significant amount of surfactant being present in the near contact region. This reflects the comparatively larger strength of the Marangoni forces. The Marangoni forces slow the rate of drainage of fluid out of the near contact region. Interestingly, this keeps the drops farther apart than the case with $Ca=0.06$. This is in stark contrast to the monotonic behavior observed for clean drops. This is investigated in more detail in next section.

4.3 Non-monotonic behavior of the minimum distance between drops

As indicated in Figs. 3-5, the minimum distance between interacting droplets may be a non-monotonic function of Ca. Here, we explore this behavior in more detail and determine the dependence of the minimum distance between drops $d_{\min}(Ca,x,h)$ on both Ca and x.

In Fig. 6, $d_{\min}(Ca,x,h)$ is plotted as a function of Ca for $x=0.3$ (solid with circles) and for $x=0$ (dashed with $*$) together with the drop morphologies at the point of closest approach. The figure indicates that for clean drops ($x=0$), $d_{\min}(Ca,x,h)$ is an increasing function of Ca. However, in the presence of surfactant, $d_{\min}(Ca,x,h)$ is non-monotonic in Ca when $x=0.3$. In particular, there is a critical value of $Ca=Ca^*\approx 0.08$ for which the near contact distance is minimized. Thus, the same distance between the drops can be achieved using two non-zero Capillary numbers (one lower and one higher). Assuming that this behavior persists for very small Capillary numbers where the film thick-

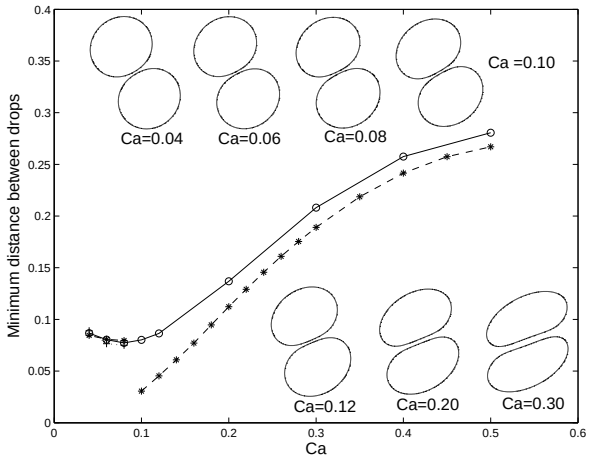

Figure 6: Minimum distances as functions of Ca. dashed-star line: clean drops ($x=0$); line with o: drops with surfactant coverage $x=0.3$. Mesh size $=1400\times1000$. Results for $x=0.3$ and $Ca=0.04$, 0.06 and 0.08 are shown for two additional mesh sizes 2100×1500 (dash-dot with $*$) and 700×500 (dotted with $+$). The drop morphologies at the critical times when $d_{\min}(Ca,x,h)$ is achieved are shown as insets.

ness reaches the scale at which van der Waals forces induce rupture, this suggests that coalescence can be achieved within a range of Capillary numbers. Note that when Ca is small, it is difficult to maintain adequate resolution in the near contact region as the drops approach one another very closely. To efficiently simulate the interaction at small Ca, adaptive mesh refinement or hybrid asymptotic/numerical methods should be used.

To validate our results around Ca^*, we have performed simulations using $N_x=2100$, $N_y=1500$ (dashed-dot with stars) as well as $N_x=700$ and $N_y=500$ (dotted with $+$). The development of a minimum is a direct consequence of the Marangoni forces. As indicated earlier, the Marangoni force resists surfactant redistribution and decreases the strength of the draining flow as the drops approach one another. When the Ca is large, this effect is dominated by the compressional force imposed by the flow and the repulsive lubrication force in the near contact region. The drops deform, dimple and remain well-separated with a distance that depends on Ca. As Ca is decreased, the strength of the Marangoni and Capillary forces increase, as shown in Fig. 10 which is described below. This results in less deformed drops with a decreased ability to drain the matrix fluid from the near contact region. At small Ca, the Marangoni flow begins to dominate in the near contact region and significantly hampers drainage which leads to larger distances between the drops. Around $Ca=Ca^*$, these effects balance and a minimum in the drop-drop distance is obtained.

To illustrate the effect of the Marangoni force, we plot in Fig. 7 the curves for the minimum distances as functions of time for three different cases: with full effect of surfactant (solid), without surfactant (clean drops, dashed) and with surfactant but without the Marangoni force (dotted). The last is accomplished by removing the Marangoni force

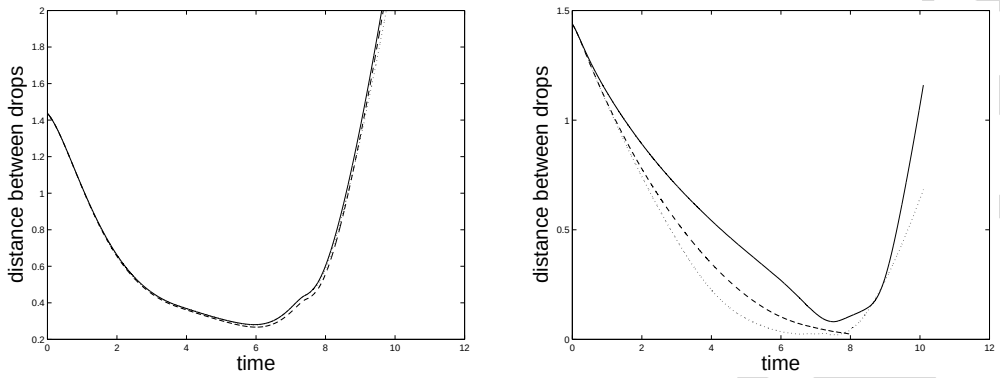

(a) (b)

Figure 7: Distance between drops as functions of time for with full effect of surfactant(solid), with surfactant without Maragoni force (dotted) and clean drops (dashed). $x=0.3$. (a) $Ca=0.50$, (b) $Ca=0.06$.

term in the Laplace-Young boundary condition (2.2) but keeping the non-uniform capillary force. When $Ca=0.5$ (a), there is little difference between the curves because the capillary force and the Marangoni force are small compared to the strength of the flow. When $Ca=0.06$ (b), there is a much bigger difference between the curves and it is clear that the Marangoni forces are responsible for the increase in the separation distance between the drops.

To gain further insight, the velocity fields induced by the Marangoni forces are plotted in Fig. 8. In particular, the velocity field with the full effect of surfactant minus the velocity field with variable Capillary force but no Marangoni force is plotted for times $6+\Delta t$ and $7+\Delta t$.

The velocity fields are obtained by using the data with full effect of surfactant at $t=6$ (or 7) as the initial data and marching one time step Δt. It can be seen that when the drops are farther apart, there is a rotational flow in the near contact region. As the drops approach one another more closely, there is a Marangoni-induced flow into the near contact region that strengthens as the drops approach one another and keeps the drops apart. As an additional point of comparison, in Fig. 9, the velocity with the full effect of surfactant minus the velocity with no surfactant is shown. From this figure, the surfactant-induced flow of fluid into the near contact region is clearly observed.

In Fig. 10, the signed magnitudes of the Marangoni $\nabla_s\sigma\cdot\boldsymbol{\tau}/Ca$ and Capillary $-\kappa\sigma/Ca$ forces are plotted at time $t=6,8$ for different Ca as functions of arclength s for the drop initially centered at $(1.7,-0.25)$. Here $\boldsymbol{\tau}$ is the unit tangent vector. Taking the normal vector to be $\mathbf{n}=(\cos\theta,\sin\theta)$, then the tangent vector $\boldsymbol{\tau}=(-\sin\theta,\cos\theta)$. The forces are interpolated to the interface positions (see Section 3) from the underlying Cartesian mesh using a cubic polynomial [44]. The location $s=0$ corresponds to the rightmost intersection of the drop interface with a horizontal line through the drop center; s increases in the counterclockwise direction. Both the Marangoni and Capillary forces are decreasing functions (in magnitude) of Ca.

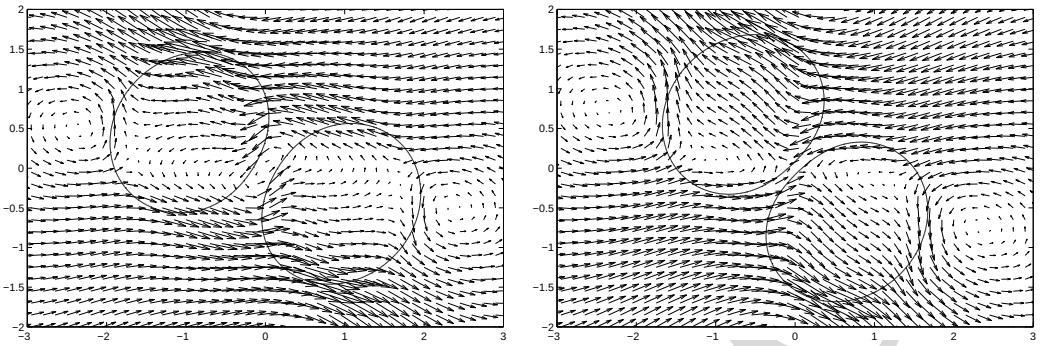

Figure 8: Velocity field with full effect of surfactant minus velocity field with surfactant without Marangoni force at times $t=6+\Delta t$ (left) and $t=7+\Delta t$ (right). $Ca=0.06, x=0.3$. Mesh size $= 1400\times1000$.

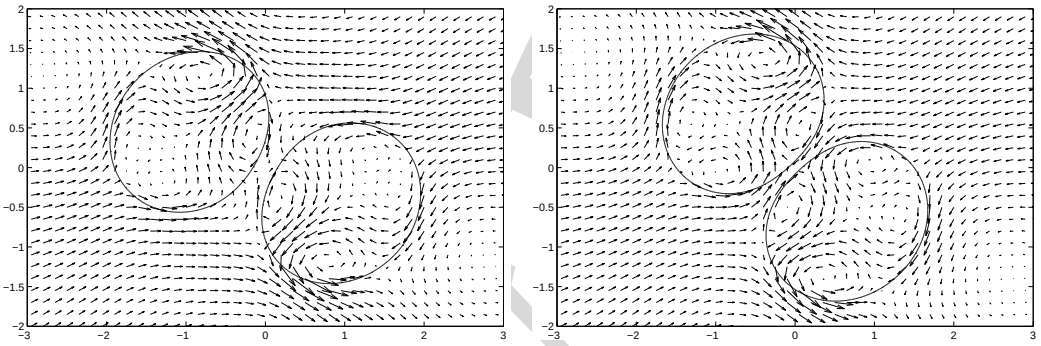

Figure 9: Velocity field with full effect of surfactant minus velocity field without surfactant at times $t=6+\Delta t$ (left) and $t=7+\Delta t$ (right). $Ca=0.06, x=0.3$. Mesh size $= 1400\times1000$.

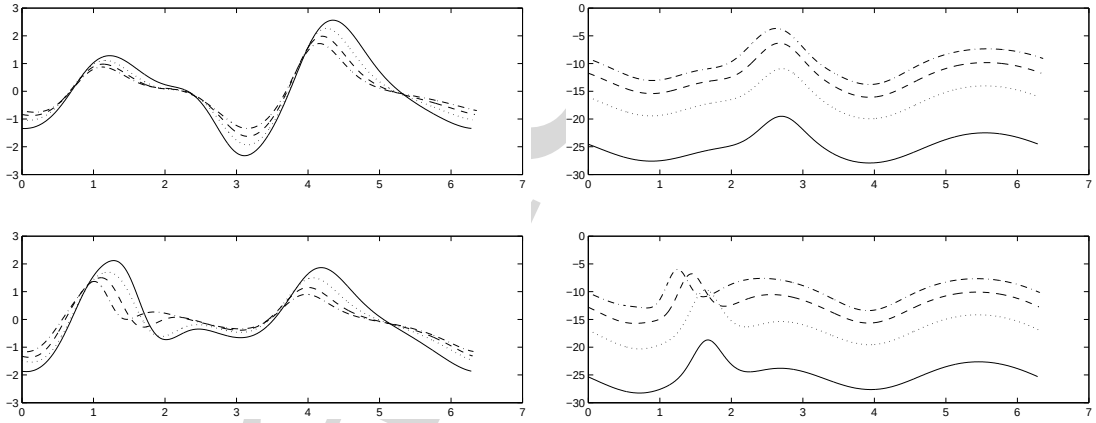

Figure 10: Signed magnitudes of Marangoni force (left) and capillary force (right) as functions of arclength at times $t=6$ (upper) and $t=8$ (lower) for various Ca and $x=0.3$. $Ca=0.04$ (solid), 0.06 (dotted), 0.08 (dashed) and 0.10 (dash-dot).

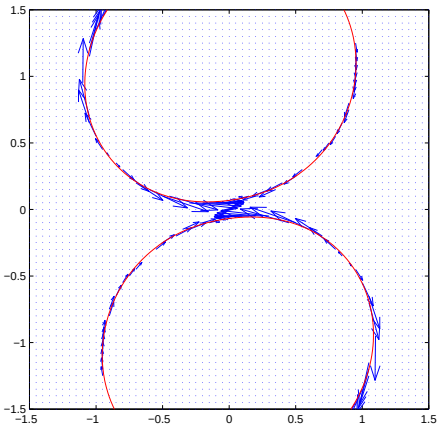

Figure 11: Marangoni force as a vector field at time $t=8$. Same setting as in Fig. 5.

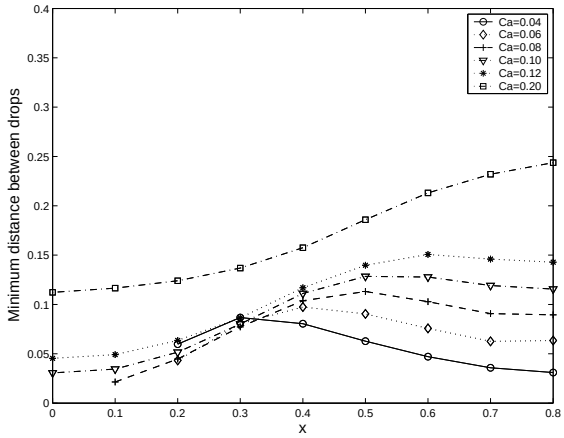

Figure 12: Minimum distances as functions of x at different Ca with mesh size 1400×1000.

The Marangoni force as a vector field is plotted at $t=8$ in Fig. 11. From Fig. 5, there are two local maximums of surfactant concentration for each drop, and correspondingly two local minimums of surface tension. In a neighborhood of each extremum point on the drop the Marangoni force is generated and points away from the extremum point. In particular, Fig. 11 clearly shows that in the near contact region the Marangoni force points to the center of the thin film and induces a flow that resists drop coalescence.

Next, consider the effect of surfactant coverage x. In Fig. 12, the minimum distance $d_{\min}(Ca,x,h)$ is plotted as a function of x for different Ca. Observe that for large Ca (e.g., $Ca=0.2$), $d_{\min}(Ca,x,h)$ is an increasing function of x. However, when Ca is decreased below a critical threshold, $d_{\min}(Ca,x,h)$ becomes a non-monotonic function of x. In particular, for small x, the minimum distance increases with increasing coverage. However, at a critical value x^*, a maximum is reached and thereafter, $d_{\min}(Ca,x,h)$ decreases as x increases. The critical coverage x^* is an increasing function of Ca.

Similar behavior was also observed experimentally by Leal and co-workers [12,15,19, 47]. For small Ca, as x increases, the drops are less deformed, their interfaces are more immobilized by the high concentration of surfactant, and it becomes easier to drain the fluid out of the near contact region thereby enabling the drops to become closer to one another. At x^*, these effects balance creating the maximum.

Remark 4.1. When both Ca and x are small, the drops approach one another very closely and large gradients may develop. This makes simulations using a uniform mesh, such as used here, very expensive and thus effectively limited the parameters we were feasibly able to simulate. Further work should use alternative approaches such as adaptive mesh refinement or asymptotic methods to overcome this difficulty.

4.4 Non-monotonic behavior of hydrodynamic diffusion

Another measure of the drop separation is the difference δy in the y-coordinates of the drop centroids. Let (x_1,y_1) and (x_2,y_2) be the centroids of two drops initially centered at $(-1.7,0.25)$ and $(1.7,-0.25)$ respectively. Define $\delta x = x_1 - x_2$ and $\delta y = y_1 - y_2$. The difference between the initial δy and the final δy after interaction and separation is a measure of the so-called hydrodynamic diffusion (e.g., [24]). That is, through hydrodynamic interactions, drops become more widely spaced than they were initially, mimicking the effects of diffusion.

In Fig. 13(a) and (b), δy is plotted versus δx for $Ca = 0.06$ and different surfactant coverages x. When $x \le 0.4$, δy is an increasing function of x for each fixed δx. For larger $x(>0.4)$, there is a transition in behavior when drops are near contact and δy becomes a decreasing function of x (e.g., see the behavior near $\delta x \approx 0$). Thus, more surfactants tend to increase the hydrodynamic diffusion for $x \le 0.4$. This is because in this regime the addition of surfactant keeps the drops farther apart (recall Fig. 12), making them rotate

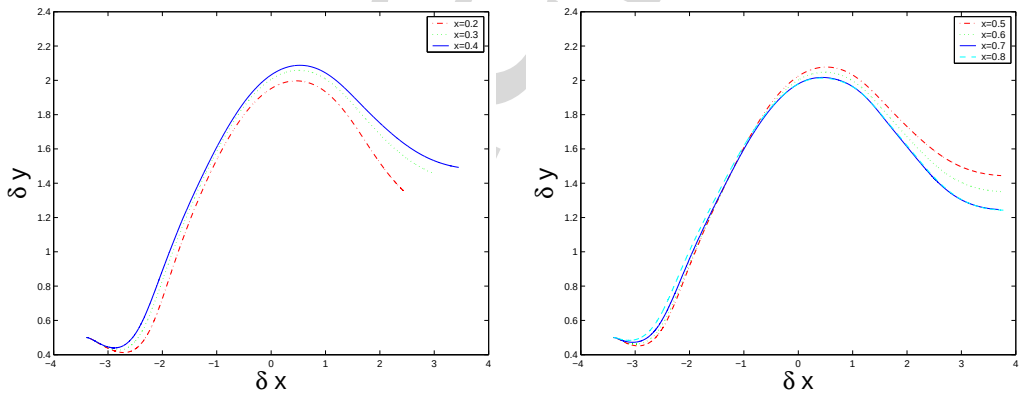

(a) (b)

Figure 13: Hydrodynamic diffusion δy versus δx for $Ca = 0.06$ and various coverages x. (a) $x \le 0.4$; (b) $x > 0.4$.

more around each other and more susceptible to transport away from each other by the shear flow.

When $x > 0.4$, the opposite occurs and hydrodynamic diffusion is reduced. This non-monotonicity is made more clear in Fig. 14 where the maximum δy is plotted as a function of x for different Ca. The corresponding values of δx are also shown.

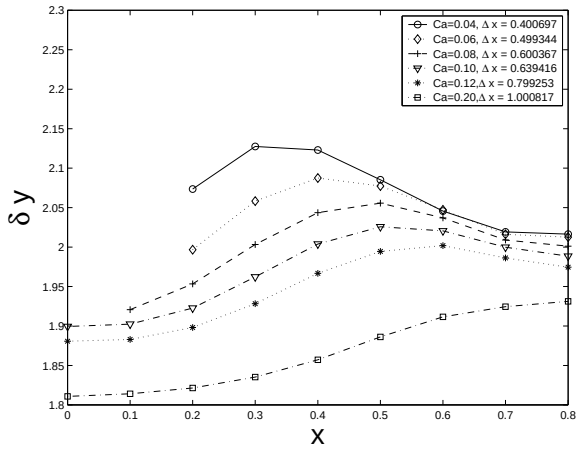

Figure 14: Hydrodynamic diffusion for $Ca = 0.06$. Maximum δy as a function of x for various Ca.

5 Conclusions and future work

In this paper, we have investigated the interaction of two, equally-sized surfactant-laden drops in shear flow in 2D. The surfactant is immiscible with the bulk fluids and the viscosity of the matrix and drop fluids are matched. The numerical algorithm is highly accurate and does not smear out the jump in the normal stress.

We have found that surfactant plays a critical and nontrivial role in drop-drop interactions. In particular, we observed non-monotonic behavior, which does not occur for clean drops, due to the presence of Marangoni forces along the interface. For example, when the Capillary number Ca was large (strong shear flow), the drops deformed significantly and the minimum distance between the drops was an increasing function of the surfactant coverage x. As Ca was decreased, a critical value of Ca emerged such that the minimum distance is a non-monotonic function of x for Ca less than this critical value. For small x, the minimum distance between the drops increased with increasing x. However, at a critical value of coverage x^*, a maximum was reached and for $x > x^*$, the minimum distance decreases with increasing x. The critical coverage x^* was found to be an increasing function of Ca. In addition, at a given surfactant coverage, the minimum distance between drops itself has a minimum at a critical Capillary number. Thus, the same distance between the drops can be achieved using two non-zero Capillary numbers (one lower and one higher). Assuming that this behavior persists for very small Capillary

numbers where the film thickness reaches the scale at which van der Waals forces induce rupture, this suggests that coalescence can be achieved within a range of Capillary numbers. A similar behavior was observed in recent experiments of drop-drop interactions by Leal and co-workers [12, 15, 19, 47].

The results presented herein have important implications for flow processing as surfactants are often used to generate desired drop size distributions in emulsions. Although our study is two-dimensional, we believe that drop-drop interactions in three-dimensional flows should be qualitatively similar as the Maragoni forces in the near contact region in 3D should have a similar effect, although the fluid in the near contact region has another dimension through which it can drain.

In the future we will generalize our algorithm to simulate drop and matrix fluids with different viscosities, three-dimensional flows and soluble surfactants.

Acknowledgments

The authors are grateful to one of the referees for careful reading of the manuscript and insightful comments, which led to the current presentation including Fig. 11. J. Xu was formerly at Department of Mathematics, University of California Irvine, Irvine, CA 92697, USA. J. X. acknowledges partial support by a research fund from Xiangtan University. Z. Li was partially supported by US ARO grants 56349-MA, AFSOR grant FA9550-09-1-0520, and NSF grant DMS-0911434. J. Lowengrub acknowledges the support of the National Science Foundation, Division of Mathematical Sciences. H. Zhao is partially supported by NSF grant DMS0811254.

References

[1] S. Adami, X. Hu and N. Adams, A conservative SPH method for surfactant dynamics, J. Comput. Phys., 229 (2010), 1909–1926.

[2] I. B. Bazhlekov, P. D. Anderson and H. E. H. Meijer, Numerical investigation of the effect of insoluble surfactants on drop deformation and breakup in simple shear flow, J. Coll. Int. Sci., 298 (2006), 369.

[3] A. Chesters, The modelling of coalescence processes in fluid liquid dispersions–a review of currrent understanding, Trans. Inst. Chem. Eng., 69 (1991), 259.

[4] A. K. Chesters and I. B. Bazhlekov, Effect of insoluble surfactants on drainage and rupture of a film between drops interacting under a constant force, J. Coll. Int. Sci., 230 (2000), 229.

[5] V. Cristini, J. Blawzdziewicz and M. Loewenberg, Near-contact motion of surfactant-covered shperical drops, J. Fluid. Mech., 11 (1998), 251.

[6] V. Cristini, J. Blawzdziewicz and M. Loewenberg, An adaptive mesh algorithm for evolving surfaces: simulations of drop breakup and coalescence, J. Comput. Phys., 168 (2001), 445–463.

[7] B. Dai and L. G. Leal, Mechanism of surfactant effects on drop coalescence, Phys. Fluids., 19 (2008), 023102.

[8] M. A. Drumwright-Clarke and Y. Renardy, The effect of insoluble surfactant at dilute concentration on drop breakup under shear with inertia, Phys. Fluids., 16 (2004), 14–21.
[9] C. D. Eggleton, T.-M. Tsai and K. J. Stebe, Tip streaming from a drop in the presence of surfactants, Phys. Rev. Lett., 87 (2001), 048302.
[10] S. Ganesan and L. Tobiska, A coupled arbitrary Lagrangian-Eulerian and Lagrangian method for computation of free surface flows with insoluble surfactants, J. Comput. Phys., 228 (2009), 2859–2873.
[11] M. Hameed, M. Siegel, Y.-N. Young, J. Li, M. R. Booty and D. T. Papageorgiou, Influence of insoluble surfactant on the deformation and breakup of a bubble or thread in a viscous fluid, J. Fluid. Mech., 594 (2008), 307–340.
[12] Y. T. Hu, D. J. Pine and L. G. Leal, Drop deformation, breakup, and coalsecence with compatibilizer, Phys. Fluids., 12 (2000), 484–489.
[13] A. J. James and J. Lowengrub, A surfactant-conserving volume-of-fluid method for interfacial flows with insoluble surfactant, J. Comput. Phys., 201 (2004), 685–722.
[14] G.-S. Jiang and D. Peng, Weighted ENO schemes for Hamilton-jacobi equations, SIAM J. Sci. Comput., 21 (2000), 2126–2143.
[15] J. W. Ha, Y. Yoon and L. G. Leal, The effect of compatibilizer on the coalescence of two drops in flow, Phys. Fluids., 15 (2003), 849–867.
[16] S. M. Khatri, A Numerical Method for Two-Phase Flows with Insoluble and Soluble Surfactant, PhD thesis, Courant Institute, NYU, 2009.
[17] M.-C. Lai, Yu-Hau Tseng and Huaxiong Huang, An immersed boundary method for interfacial flows with insoluble surfactant, J. Comput. Phys., 227 (2008), 7279–7293.
[18] L. D. Landau and E. M. Lifshitz, Fluid Mechanics, Pergamon press, 1958.
[19] L. G. Leal, Flow induced coalecsence of drops in a viscous fluid, Phys. Fluids., 16 (2004), 1833–1851.
[20] J. Lee and C. Pozrikidis, Effect of surfactants on the deformation of drops and bubbles in Navier-Stokes flow, Comput. Fluids., 35 (2006), 43–60.
[21] R. LeVeque and Z. Li, The immersed interface method for elliptic equations with discontinuous coefficients and singular sources, SIAM J. Numer. Anal., 31 (1994), 1019–1044.
[22] R. LeVeque and Z. Li, Immersed interface methods for Stokes flow with elastic boundaries or surface tension, SIAM. J. Sci. Comput., 18 (1997), 709–735.
[23] X. Li and C. Pozrikidis, Effect of surfactants on drop deformation and on the rheology of dilute emulsion in Stokes flow, J. Fluid. Mech., 385 (1999), 79–99.
[24] M. Loewenberg and E. J. Hinch, Collision of two deformable drops in shear flow, J. Fluid. Mech., 388 (1997), 299–315.
[25] J. Lowengrub, J. Xu and A. Voigt, Surface phase separation and flow in a simple model of multicomponent drops and vesicles, Fluid. Dyn. Mater. Proc., 3 (2007), 1–19.
[26] S. Lyu, T. D. Jones, F. S. Bates and C. W. Macosko, Role of block copolymers on suppression of droplet coalescence, Macormolecules, 35 (2002), 7845–7855.
[27] P. Macklin and J. Lowengrub, Evolving interfaces via gradients of geometry-dependent interior poisson problems: application to tumor growth, J. Comput. Phys., 203 (2005), 191–220.
[28] W. J. Milliken, H. A. Stone and L. G. Leal, The effect of surfactant on transient motion of newtonian drops, Phys. Fluids. A., 5 (1993), 69–79.
[29] S. T. Milner and H. Xi, How copolymers promote mixing of immiscible homopolymers, J. Rheol., 40 (2000), 663–687.
[30] M. Muradoglu and G. Tryggvason, A front-tracking method for the computation of interfacial flows with soluble surfactants, J. Comput. Phys., 227 (2008), 2238–2262.

[31] S. Osher and R. P. Fedkiw, Level set methods: an overview and some recent results, J. Comput. Phys., 169 (2001), 463–502.
[32] S. Osher and J. A. Sethian, Fronts propagating with curvature dependent speed: algorithms based on Hamilton-Jacobi formulations, J. Comput. Phys., 79 (1988), 12–49.
[33] Y. Pawar and K. J. Stebe, Marangoni effects on drop deformation in an extensional flow: the role of surfactant physical chemistry I: insoluble surfactants, Phys. Fluids., 8 (1996), 1738–1751.
[34] J. A. Sethian and P. Smereka, Level set methods for fluid interfaces, Ann. Rev. Fluid. Mech., 35 (2003), 341–372.
[35] C.-W. Shu, Total-variation-diminishing time discretization, SIAM J. Sci. Stat. Comput., 9 (1988), 1073–1084.
[36] M. Sussman, P. Smereka and S. Osher, A level-set approach for computing solutions ot incompressible two-phase flow, J. Comput. Phys., 114 (1994), 146–159.
[37] H. A. Stone, A simple derivation of the time-dependent convective-diffusion equation for surfactant transport along a deforming interface, Phys. Fluids. A., 2 (1989), 111.
[38] H. A. Stone and L. G. Leal, The effects of surfactants on drop deformation and breakup, J. Fluid. Mech., 220 (1990), 161–186.
[39] S. Tasoglu, U. Demirci and M. Muradoglu, The effect of soluble surfactant on the transient motion of a buoyancy-driven bubble, Phys. Fluids., 20 (2008), 04085.
[40] K. E. Teigen, P. Song, J. Lowengrub and A. Voigt, A diffusive-interface method for two-phase flows with soluble surfactants, J. Comput. Phys., in review.
[41] H. Wong, D. Rumschitzki and C. Maldarelli, On the surfactant mass balance at a deforming fluid interface, Phys. Fluids., 8 (1996), 3203–3204.
[42] J. Xu and H. Yuan, Three dimensional level-set approach for surfactant convection-diffusion equation along a moving interface, submitted.
[43] J. Xu, Y. Yang and J. Lowengrub, A level-set continuum method for two-phase flows with insoluble surfactant, submitted.
[44] J. Xu, Z. Li, J. Lowengrub and H. Zhao, A level set method for solving interfacial flows with surfactant, J. Comput. Phys., 212 (2006), 590–616.
[45] J. Xu and H. Zhao, An Eulerian formulation for solving partial differential equations along a moving interface, J. Sci. Comput., 19 (2003), 573–594.
[46] X. Yang and A. J. James, An arbitrary Lagrangian-Eulerian (ALE) method for interfacial flows with insoluble surfactants, Fluid. Dyn. Mater. Proc., 3 (2007), 65–96.
[47] Y. Yoon, A. Hsu and L. G. Leal, Experimental investigation of the effects of copolymer surfactants on flow-induced coalescence of drops, Phys. Fluids., 19 (2007), 023102.
[48] J. Zhang, D. M. Eckmann and P. S. Ayyaswamy, A front tracking method for a deformable intravascular bubble in a tube with soluble surfactant transport, J. Comput. Phys., 214 (2006), 366–396.
[49] H. Zhao, T. F. Chan, B. Merriman and S. Osher, A variational level set approach to multiphase motion, J. Comput. Phys., 127 (1996), 179–195.